

Science Arts & Métiers (SAM)

is an open access repository that collects the work of Arts et Métiers ParisTech researchers and makes it freely available over the web where possible.

This is an author-deposited version published in: <http://sam.ensam.eu>
Handle ID: <http://hdl.handle.net/10985/7414>

To cite this version :

Nicolas SAINTIER, Thierry PALIN-LUC, Jérôme BÉNABÈS, Francis COCHETEUX - Non-local energy based fatigue life calculation method under multiaxial variable amplitude loadings - International Journal of Fatigue - Vol. 54, p.68-83 - 2013

Any correspondence concerning this service should be sent to the repository

Administrator : archiveouverte@ensam.eu

Non-local energy based fatigue life calculation method under multiaxial variable amplitude loadings

Nicolas Saintier^{a,b,c,*}, Thierry Palin-luc^{a,b,c}, Jérôme Bénabes^{a,b,c}, Francis Cocheteux^d

^aArts et Metiers ParisTech, I2M, UMR 5295, F-33400 Talence, France

^bUniv. Bordeaux, I2M, UMR 5295, F-33400 Talence, France

^cCNRS, I2M, UMR 5295, F-33400 Talence, France

^dAgence d'Essai Ferroviaire – SNCF, 21, Avenue du Président Allende, 94407 Vitry-Sur-Seine, France

A B S T R A C T

Reliable design of industrial components against high cycle multiaxial fatigue requires a model capable of predicting both stress gradient and load type effects. Indeed, taking into account gradient effects is of prior importance for the applicability of fatigue models to real structures. In this paper, a fatigue life assessment method is proposed for proportional and non-proportional multiaxial variable amplitude loadings in the range 10^4 – 10^7 cycles. This method derives from the fatigue criterion initially proposed by Palin-Luc and Lasserre (1998) [2] and revisited by Banvillet et al. (2003) [16] for multiaxial constant amplitude loading. The new proposal consists of a complete reformulation and extension of the previously cited energy based fatigue strength criteria. It includes two major improvements of the existing criteria. The first one consists in a fatigue criterion for multiaxial variable amplitude loadings while only constant amplitude loadings were considered in the above cited works. The second one is an extension to an incremental fatigue life assessment method for proportional and non-proportional multiaxial variable amplitude loadings. No cycle counting technique is needed whatever the variable amplitude loadings type considered (uniaxial or multiaxial). The predictions of the method for constant and variable amplitude multiaxial loadings are compared with experimental results on specimens from literature and from new experiments on a ferrite-perlitic steel. The above mentioned method has been implemented as a post-processor of a finite element software. An application to a railway wheel is finally presented.

Keywords:

High cycle fatigue
Fatigue life calculation method
Multiaxial
Energy
Gradient

1. Introduction

Designing metallic components against variable amplitude multiaxial fatigue loadings is still a difficult problem to handle for engineers. The two major difficulties can be summarized as follows. The fatigue life assessment method has to catch the full complexity of in service loadings (variable amplitude, non-proportional multiaxial loadings, etc.) [1] and to account for well known stress/strain gradient effects often encountered on real structures [2–4].

High cycle multiaxial fatigue strength criteria have been developed for over 50 years resulting in a large variety of formulations usually based on a combination of strain, stress or strain energy quantities [5]. Since the pioneer work of Jasper [6] in 1923 who used an energy based quantity to analyze tension–compression loadings, energy based formulations have been strongly developed. Ellyin [7,8] showed that a combination of both the plastic and

elastic strain work could be efficiently used as damage parameter in multiaxial fatigue. In their review on energy based multiaxial fatigue life criteria, Macha and Sonsino [9] showed that energy based formulations are good candidates when dealing with loadings presenting complex temporal histories.

Energy based approaches have other advantages when dealing with variable amplitude loadings.

- In general, the extension of a multiaxial fatigue life assessment method to the variable amplitude domain necessitates the use of particular cycle counting techniques in order to extract, from a stress tensor time evolution with variable amplitude, clearly identified load cycles for which any damage parameter could be computed.
- Although there are a lot of cycle counting techniques, none is unanimously recognized especially under non-proportional multiaxial stress states [10].
- The choice of the cycle counting algorithm is important since it influences the result of the calculated fatigue life [10,11].

* Corresponding author at: Arts et Metiers ParisTech, I2M, UMR 5295, Esplanade des Arts et Métiers, F-33400 Talence, France. Tel.: +33 687209481.

E-mail address: nicolas.saintier@ensam.eu (N. Saintier).

Nomenclature

dT	triaxiality degree of stresses	ν	Poisson ratio
\vec{n}	unit vector normal to a material plane	$\overline{\varpi}_g$	mean value over V^* of the damaging part of W_g
r	radius in cylindrical coordinates	$\overline{\varpi}_g^D$	threshold value of $\overline{\varpi}_g$ at the endurance limit
t	time	$\overline{\varpi}_{g,Ten}$	expression of $\overline{\varpi}_g$ in tension
A	fracture elongation in tension	$\overline{\varpi}_{g,RotBen}$	expression of $\overline{\varpi}_g$ in rotating bending
C_i	fatigue critical point	$\overline{\varpi}_{g,PB}$	expression of $\overline{\varpi}_g$ in plane bending
C_s	safety factor	σ_a	normal stress amplitude
E	Young modulus	σ_{eq}	fatigue indicator predictor for multiaxial fatigue life criterion
$F(dT, \beta)$	correction function depending on the triaxiality degree of stresses	σ_H	hydrostatic stress
N_{exp}, N_{sim}	experimental and simulated fatigue lives respectively expressed in cycles	$\overline{\sigma}$	mean normal stress
R_σ, R_τ	load ratio $\sigma_{min}/\sigma_{max}$ or τ_{min}/τ_{max}	σ^*	threshold stress below which there is no micro-damage initiation
R_m	maximum tensile strength	$\sigma_{Ten,-1}^D$	endurance limit in fully reversed tension-compression
$\underline{\underline{\sigma}}(M, t)$	deviatoric part of the stress tensor at point M function of time	$\sigma_{RotBen,-1}^D$	endurance limit in fully reversed rotating bending
T	loading period or duration of a variable amplitude loading sequence	$\sigma_{PB,-1}^D$	endurance limit in fully reversed plane bending
T_{exp}, T_{sim}	experimental and simulated fatigue lives respectively expressed in time	$\sigma_{Tor,-1}^D$	endurance limit in fully reversed torsion
V^*	volume influencing fatigue crack initiation	σ_Y, τ_Y	yield stress in tension, in torsion respectively
W_g	strain work density given to the material on a loading period or sequence	τ_a	shear stress amplitude
W_g^*	threshold value of W_g corresponding to σ^*	$\overline{\tau}$	mean shear stress
β	material parameter of the volumetric energy based proposal	τ_{-1}^D	endurance limit in fully reversed torsion
$\underline{\underline{g}}(M, t)$	strain tensor at point M function of time	ϕ	phase shift for combined loadings
		$\underline{\underline{\sigma}}(M, t)$	stress tensor at point M function of time
		\cdot	double contracted product $\underline{\underline{X}} : \underline{\underline{Y}} = \sum_{ij} X_{ij} Y_{ij}$

- For multiaxial non-proportional stress states, in many approaches found in the literature, the variable chosen for cycle counting differs from the damage parameter of the fatigue life assessment method [12].
- Compared to stress or strain based critical plane approaches, another advantage of an energy based criterion is that it can easily be written in an incremental form avoiding the use of cycle counting algorithm. This paper will present such an approach.

The influence of stress and strain gradients on the fatigue strength is now well reported in the literature, but components have seldom a well defined notch factor. Consequently, the use of data from laboratory tests has to be done very carefully [2–4,13] when applied to real components. Furthermore, in high cycle fatigue, the influence of the load type on the fatigue strength is well known (endurance limits in tension-compression and in bending are different). An optimized design against fatigue requires a method able to consider both the volumetric distribution of stresses and strains and the load type effect; the proposed method considers such volumetric distributions.

2. Fatigue life assessment method

In the high cycle fatigue regime it is generally assumed that negligible macroscopic plastic strains occur and that elastic shakedown hypothesis is reasonable. Since this paper is devoted to the field of endurance or limited endurance (i.e. 10^5 – 10^7 cycles) this hypothesis is considered. Consequently, only the elastic part of the total strain energy will be considered hereafter.

The present proposal derives from the work of Froustey and Lasserre [14], Palin-Luc and Lasserre [2] and Banville [11]. The new proposal consists of a complete reformulation and extension of the previously cited energy based fatigue strength criteria: it proposes non-local energy based multiaxial fatigue life criteria

expressed in an incremental form that is suitable for non-proportional variable amplitude loadings. Furthermore, an extension to an incremental fatigue life assessment method for multiaxial variable amplitude loadings is proposed.

2.1. An energy parameter

The proposed damage parameter is based on two main hypothesis:

1. As already noticed, the fatigue damage parameter is computed after macroscopic elastic shakedown. This hypothesis is justified because our proposal lies within the high cycle fatigue regime (elastic shakedown is supposed to be reached after a few thousands cycles [15]).
2. The strain work density given to the material is considered as the driving force for fatigue crack initiation.
3. A volumetric approach is developed based on a sequence length dependant energy threshold (see Section 2.3)

Ellyin [7] underlined that the strain work can be calculated as the sum of elastic and plastic strain works, so that the total, $W(M, t)$, the elastic, $W^e(M, t)$, and the plastic, $W^p(M, t)$ strain work densities are related by:

$$W(M, t) = W^e(M, t) + W^p(M, t) \quad (1)$$

According to the first previous hypothesis the volumetric strain energy density is given by the following equation where the plastic strain energy is neglected.

$$W(t, M) = \frac{1}{2} \underline{\underline{\sigma}}(M, t) : \underline{\underline{g}}(M, t) = \frac{1}{2} \sigma_{ij}(M, t) \varepsilon_{ij}(M, t) \quad (2)$$

$\sigma_{ij}(M, t)$ (resp. $\varepsilon_{ij}(M, t)$) denotes the temporal evolution of the ij term of the stress (resp. elastic strain) tensor at a material point M . It is assumed that the strain work density given to the material

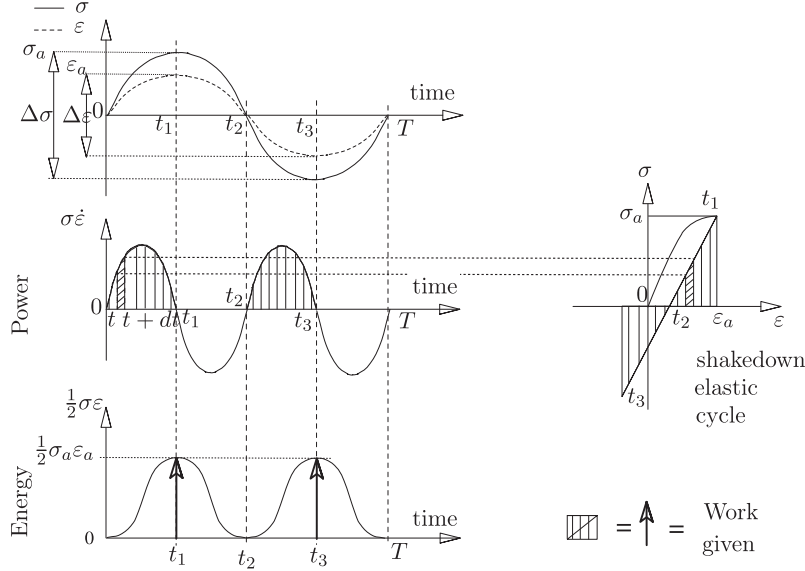


Fig. 1. Illustration of work and elastic strain power given to an elementary volume element, during a loading period T (with the assumption of elastic shakedown) under fully reversed tension.

is the relevant mechanical parameter to compute a fatigue damage indicator. This concept is illustrated Fig. 1 for fully reversed uniaxial stress state (tension compression). During the tensile part of the loading, when the power is positive, the strain work density is considered as being given to the material. On the contrary, in the relaxing phase when the strain power is negative, the material restitutes the strain energy. It is considered that no damage occurs during this phase. For multiaxial loading the situation is more complex in particular due to mean stress/strain and Poisson effects. Fig. 2 illustrates the situations where the strain work density is considered as being given to the material.

As said in the introduction section, to avoid the use of any cycle counting method, an incremental definition of the damage parameter is chosen. From this analyses it results the general form for the increment of strain work density, dW_g , given to an elementary volume dv , at time t :

$$dW_g(M, t) = \sum_{ij} dW_{g,ij}(M, t) \quad (3)$$

$$dW_g(M, t) = \sum_{ij} \langle \sigma_{ij}(M, t) \dot{\epsilon}_{ij}(M, t) \text{sign}(\dot{\epsilon}_{ij}(M, t) \dot{\sigma}_{ij}(M, t)) \rangle dt$$

- $\sigma_{ij}(M, t)$ and $\epsilon_{ij}(M, t)$ are the stress and elastic strain tensor components at M and function of time.
- $\dot{\epsilon}_{ij}(M, t)$ and $\dot{\sigma}_{ij}(M, t)$ are the stress and elastic strain rate tensor components at M and function of time.

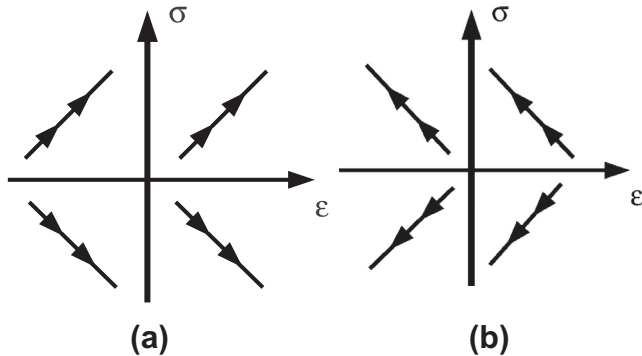


Fig. 2. Elastic strain stress paths that corresponds to a positive values of the strain work density increment.

- $\langle \cdot \rangle$ represents the Macaulay brackets ($\langle x \rangle = x$ if $x > 0$; $\langle x \rangle = 0$ if $x \leq 0$).

The strain energy density given to the material over a loading period T (or sequence of duration T for variable amplitude loading) is then:

$$W_g(M) = \int_t^{t+T} dW_g(M, t) \quad (4)$$

2.2. Multiaxial stress states

Stress triaxiality sensitivity is a major feature in multiaxial fatigue that strongly depends on the considered material. Such sensitivity can hardly be directly related to some simple mechanical properties so that it is usually introduced empirically in the formulations. To take into account the material sensitivity to the stress triaxiality we define at each material point M , a triaxiality parameter as follows:

$$dT(M, t) = \frac{W^s(M, t)}{W(M, t)} \quad \text{if } W(M, t) \neq 0, \quad \text{otherwise } dT(M, t) = 0 \quad (5)$$

where $W(M, t)$ (resp. $W^s(M, t)$) is the instantaneous total (resp. spherical) elastic strain energy. $W^s(M, t)$ is defined by:

$$W^s(M, t) = 1/6(\text{trace}(\sigma(M, t))\text{trace}(\epsilon(M, t))) = \frac{1}{2} \sigma_{ij}^s \epsilon_{ij}^s \quad (6)$$

where s denotes the spherical part of the stress and elastic strain tensors.

Based on previous studies [2,16], we propose to take into account the material sensitivity to the triaxiality of stresses by using an empirical function, $F(dT(M), \beta)$, where dT is the triaxiality degree of stresses and β a material parameter. This function (Eq. (7)) was identified using a large multiaxial fatigue database (see [17] for more details). For a given material this function represents the evolution, versus dT , of the ratio of the strain work density value at the endurance limit, noted W_g^D , and its value in torsion $W_{g,tors}^D$. It has been built so that $F(dT(M), \beta) = 1$ in torsion for any material.

$$F(dT(M), \beta) = \frac{W_g^D}{W_{g,tors}^D} = \frac{1}{1 - dT(M)} \left[1 - \frac{1}{\beta} \ln [1 + dT(M)(e^\beta - 1)] \right] \quad (7)$$

As a consequence, at the endurance limit, whatever the loading and the stress state, W_g^D is related to its value in torsion, $W_{g,tors}^D$, and under simple uniaxial stress state, $W_{g,uniax}^D$, by the following relations:

$$W_g^D(M) = W_{g,tors}^D F(dT(M), \beta) \quad (8)$$

So that under uniaxial loading,

$$W_{g,uniax}^D = W_{g,tors}^D F(dT_{uniax}(M), \beta) \quad (9)$$

For any cyclic stress state with a triaxiality degree dT , it is then possible to compute, at the endurance limit, the strain work density given to the material which is equivalent to a uniaxial stress state. Such an equivalent strain work density is defined by Eq. (10). Considering the triaxiality degree of stresses at a point M , this is – at the endurance limit – the bearable strain work density given to the material per load cycle which is equivalent to the given strain work density that the same material accepts at the endurance limit under a uniaxial cyclic stress state.

$$W_{g,eq}(M) = \frac{F(dT_{uniax}(M), \beta)}{F(dT(M, t), \beta)} W_g^D(M) \quad (10)$$

Considering now the incremental definition (Eq. (3)), an incremental equivalent strain energy parameter is proposed by the following equation with the same F function but where dT is time dependent.

$$dW_{g,eq}(M, t) = \frac{F(dT_{uniax}(M), \beta)}{F(dT(M, t), \beta)} dW_g(M, t) \quad (11)$$

Combing Eqs. (4) and (11) we obtain the total given strain work density during a load period T (or sequence of duration T for variable amplitude loadings), equivalent to a uniaxial stress state:

$$W_{g,eq}(M) = \int_T dW_{g,eq}(M, t) \quad (12)$$

Whatever the loading (constant or variable amplitude) the proposed mutiaxial fatigue criterion is then simply expressed as follows:

$$W_{g,eq}(M) \leq W_{g,uniax}^D \quad (13)$$

where $W_{g,uniax}^D$ is the bearable strain work density under uniaxial loading at the endurance limit given by:

$$W_{g,uniax}^D = \frac{(\sigma_{Tens,-1}^D)^2}{E} \quad (14)$$

where $\sigma_{Tens,-1}^D$ is the endurance limit on smooth specimens under fully reversed tension–compression.

2.3. Damage parameter

From fully reversed fatigue experiments on spheroidal graphite cast iron, Palin-Luc et al. [18] have shown that a threshold stress, σ^* , can be defined below the conventional endurance limit¹ σ^D . At a considered point, a stress amplitude lower than this threshold does not initiate observable damage at the microscale (no microcrack). A stress amplitude between σ^* and σ^D contributes to micro-damage initiation only, which could develop if, in the course of time, there is a stress amplitude higher than σ^* . The stress limit σ^* is considered as a threshold stress of no damage initiation at the microscale, whereas the usual endurance limit σ^D corresponds to a macrocrack initiation threshold.

¹ The endurance limit is considered as the asymptotic tendency of the S-N curve observed at 10^7 or more cycles according to many standards. The aim of this paper is not to predict an infinite life but fatigue life in HCF regime. It is now often considered that infinite fatigue life may not exist for many alloys [19].

Banville [11] expressed this threshold concept in terms of an energy limit, W_g^* , representing the minimum strain work volumetric density (per load cycle) necessary to create, after a high number of cycles, an irreversible damage in a representative elementary volume (REV).

For constant amplitude loading, the damaging part of the strain work density can be simply expressed by:

$$W_{g,eq,dam}(M) = \langle W_{g,eq}(M) - W_g^* \rangle \quad (15)$$

where the symbol $\langle \cdot \rangle$ represent the Macaulay brackets. Considering a uniaxial loading case, it is easily shown [20] that:

$$\sigma^* = \sqrt{2(\sigma_{-1,Tens.}^D)^2 - (\sigma_{-1,Rot.Bend.}^D)^2} \quad (16)$$

$$W_g^* = \frac{(\sigma^*)^2}{E} \quad (17)$$

where $\sigma_{-1,Tens.}^D, \sigma_{-1,Rot.Bend.}^D$ are the endurance limits of the material obtained on smooth specimens under fully reversed tension and rotating bending respectively. $W_{g,eq,dam}(M)$ corresponds to the difference by excess between the strain work given to the material for one loading period T , and an energy threshold quantity W_g^* . This threshold is closely related to the concept of cycle since under constant amplitude loading, W_g^* corresponds to a threshold per cycle.

If the loading is of variable amplitude, the difficulty lies primarily in the computation of the strain work part considered as damaging. Indeed, the formulation proposed Eq. (15) cannot be directly applied to any variable amplitude loadings since the $W_{g,eq}(M)$ term depends on the sequence length while the second term, W_g^* , does not.

For variable amplitude loadings, it is proposed to modify Eq. (15) as follows:

$$W_{g,eq,dam}(M) = \langle W_{g,eq}(M) - \alpha_M \cdot W_g^* \rangle \quad (18)$$

The α_M parameter is defined in the following subsection and is closely related to the temporal evolution of the stress/strain tensors and sequence duration at point M . It is equal to 1 under constant amplitude loading, and can take any positive value greater than one for variable amplitude loading.

2.3.1. Computing α_M

2.3.1.1. Uniaxial loading. For sake of simplicity, let us first consider the case of uniaxial variable amplitude loading. The signed energy function, $\xi(t)$, as proposed by [21], is introduced as follows:

$$\xi(t) = \frac{\sigma(t)\epsilon(t)}{2} \text{sign}(\sigma(t)) \quad (19)$$

where $\text{sign}(x) = 1$ if $x > 0$ and $\text{sign}(x) = -1$ if $x < 0$. This is close to the Lagoda's proposal [22,23] in the case of pur elastic regime.

Its evolution for fully reversed and alternated constant amplitude uniaxial loading is illustrated Fig. 3 together with the evolution of the cumulated strain energy density (12) given to the material. For both loading cases the cumulated strain energy evolution shows typical time sequence that consists in a plateau regime (stress relaxation) followed by an increase. Such typical time sequence will be called “transition”. For fully reversed loadings, two transitions are counted in one full cycle, while for alternated loadings there is only one transition per cycle. Variable amplitude loadings consist of a succession of transitions which number depends on the sequence length. These transitions can be considered as elementary time sequences on which the concept of energy threshold has to be transferred. To each transition an energy threshold is associated. This energy threshold is computed as follows:

$$W_{tran,M,t_k \rightarrow t_{k+1}}^* = \alpha_{M,t_k \rightarrow t_{k+1}} W_g^* \quad (20)$$

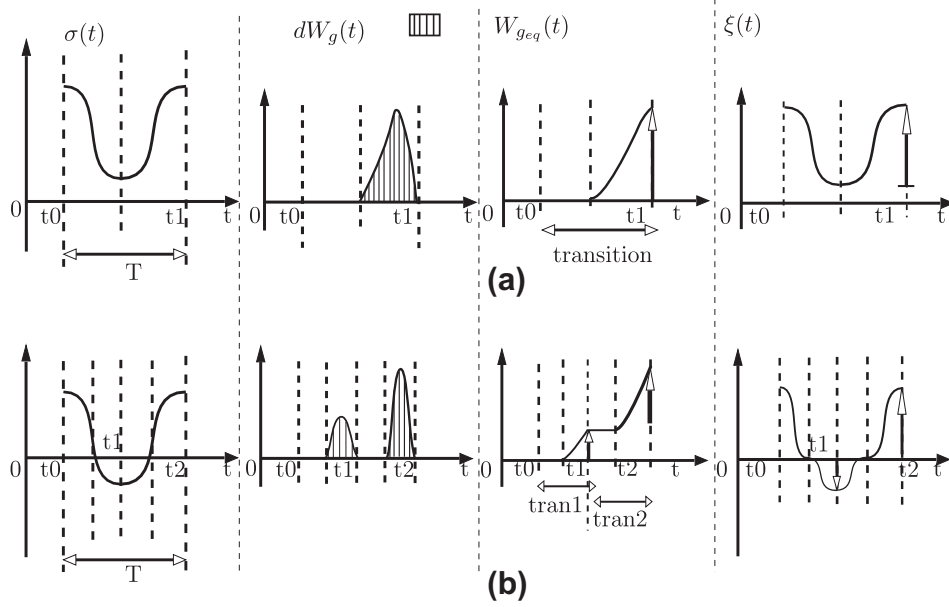


Fig. 3. Stress, incremental and cumulated damage parameter and energy function evolution under uniaxial tensile loading for positive and negative loading ratio.

where $\alpha_{M,t_k \rightarrow t_{k+1}}$ is related to the amplitude of the transition in terms of strain energy so that:

$$\alpha_{M,t_k \rightarrow t_{k+1}} = \frac{|\zeta(M, t_{k+1})|}{\left(\frac{1 - \text{sign}(\xi(M, t_k)\xi(M, t_{k+1}))}{2} \right) |\zeta(M, t_k)| + |\zeta(M, t_{k+1})|} \quad (21)$$

For sake of simplicity $\alpha_{M,t_k \rightarrow t_{k+1}}$ is noted α_{M,t_k} in the following.

For a variable amplitude loading, n being the number of transitions during the sequence, the total damaging part of the strain work density is given by:

$$W_{g_{eq,dam}}(M) = \left\langle \sum_{k=0}^{n-1} \left(\int_{t_k}^{t_{k+1}} dW_{g_{eq}}(M) - \alpha_{M,t_k} W_g^* \right) \right\rangle \quad (22)$$

$$= \left\langle W_{g_{eq}}(M) - \alpha_M W_g^* \right\rangle \quad (23)$$

with

$$\alpha_M = \sum_{k=0}^{n-1} \alpha_{M,t_k} \quad (24)$$

Under constant amplitude loading, Eq. (21) ensures that $\alpha_M = 1$ whatever the loading ratio. One can note that α_M is a sort of automatic counter of the transition number (between strain work given and released) in the time fluctuations of the strain work energy density over the loading sequence.

2.3.1.2. Multiaxial loading. Now, let us consider the most general case of multiaxial loadings where the six components of the stress and strain tensors are fluctuating in time. For sake of simplicity the engineering notations for stress and strain components is used in the following:

$$\begin{pmatrix} \sigma_{11} \\ \sigma_{22} \\ \sigma_{33} \\ \sigma_{23} \\ \sigma_{13} \\ \sigma_{12} \end{pmatrix} = \begin{pmatrix} \sigma_1 \\ \sigma_2 \\ \sigma_3 \\ \sigma_4 \\ \sigma_5 \\ \sigma_6 \end{pmatrix} \quad \text{and} \quad \begin{pmatrix} \epsilon_{11} \\ \epsilon_{22} \\ \epsilon_{33} \\ 2\epsilon_{23} \\ 2\epsilon_{13} \\ 2\epsilon_{12} \end{pmatrix} = \begin{pmatrix} \epsilon_1 \\ \epsilon_2 \\ \epsilon_3 \\ \epsilon_4 \\ \epsilon_5 \\ \epsilon_6 \end{pmatrix} \quad (25)$$

Each one of those six $\sigma_i(t)$, $\epsilon_i(t)$ time histories contributes individually to the total strain work density via $dW_{g,i}$ terms as proposed Eq. (3). Similarly to the uniaxial case, it is assumed that

the threshold W_g^* is distributed on the six $dW_{g_{eq,i}}$ terms proportionally to their contribution to the total strain work density. The proportionality factor $P_l(M)$ is given by:

$$P_l(M) = \frac{\int_T dW_{g_{eq,l}}}{W_{g_{eq}}} \quad (26)$$

It has to be noticed that $\sum_{l=1}^6 P_l = 1$. This parameter is then introduced in the formulation as follows:

$$W_{g_{eq,dam}}(M) = \left\langle \sum_{l=1}^6 \sum_{k=0}^{N-1} \int_{t_k}^{t_{k+1}} dW_{g_{eq,l}}(M) - P_l(M) \alpha_{M,l,t_k} W_g^* \right\rangle \quad (27)$$

$$= \left\langle W_{g_{eq}}(M) - \sum_{l=1}^6 P_l(M) \alpha_{M,l} W_g^* \right\rangle \quad (28)$$

$$= \left\langle W_{g_{eq}}(M) - \lambda_M W_g^* \right\rangle \quad (29)$$

with

$$\lambda_M = \sum_{l=1}^6 P_l(M) \alpha_{M,l} \quad (30)$$

Under multiaxial variable amplitude loadings in the high cycle fatigue regime, the damaging strain work density is the part in excess of the strain work density given to the material with regard to the threshold energy density $\lambda_M W_g^*$.

Furthermore, like α_M , λ_M is sequence length dependent. If a given variable amplitude multiaxial load sequence S of duration T is reproduced k times to build a new load sequence S' of duration kT , it is easily shown that we obtained:

$$\lambda_M^{S'} = k \lambda_M^S \quad (31)$$

The two representations are illustrated Fig. 4.

2.3.2. Volume influencing fatigue crack initiation V^*

When stress gradients are present, Palin-Luc and Lasserre [2] and Banville et al. [16] supposed that the threshold stress delimits a volume influencing fatigue crack initiation V^* . We keep this assumption and consider that the potentially critical points C_i (where a fatigue crack can occur) are the points around each C_i where the strain work density given to the material W_g presents a local maximum. Around each one of these potentially critical

points, the influence volume V^* is defined by all the points where the damaging work is not zero.

$$V^*(C_i) = \{\text{points } M(x,y,z) \text{ around } C_i \text{ so that } W_{g_{eq,dam}}(M) \neq 0\} \quad (32)$$

Fig. 5 schematically illustrates in 2 dimensions the V^* identification considering an arbitrary initial strain work map. The critical points correspond to the local maxima of $W_{g_{eq}}$, and the influence volumes are built around these points.

2.3.3. Volumetric damage parameter

Having considered that all the material points included in V^* have an influence in the damage process leading to fatigue crack initiation, the non-local damage parameter $\varpi_{g_{eq}}$ is defined as the volumetric average over V^* of the damaging strain work of the considered multiaxial variable amplitude loading sequence. This can be expressed as:

$$\varpi_{g_{eq,dam}}(C_i) = \frac{1}{V^*(C_i)} \int_{V^*(C_i)} W_{g_{eq,dam}} dv \quad (33)$$

For any multiaxial variable amplitude loading, there is no fatigue crack initiation if the following inequality is true:

$$\varpi_{g_{eq,dam}}(C_i) < \varpi_{g_{unimax}}^D \quad (34)$$

where $\varpi_{g_{unimax}}^D$ is the maximum volumetric average (in V^*) of the damaging strain energy density that the material can support without cracking at the endurance limit. This is identified from the

endurance limit of the material on smooth specimen under fully reversed tension, plane bending or rotating bending. (for instance, $\varpi_{g_{unimax}}^D = (\sigma_{Tens,-1}^D)^2 / E$). The proposed criterion is stress gradient dependent.

2.4. Master curve

A fatigue life calculation method is often a fatigue criterion extension Weber et al. [24], itself based on a damage parameter. In a fatigue criterion, the damage parameter threshold is fixed for one fatigue life. This one generally corresponds to the endurance limit of the material that is experimentally identified at 10^6 or 10^7 cycles for example. In some cases, fatigue criteria can be used to propose more general fatigue life calculation method by empirically linking the value of the damage parameter to the fatigue life, keeping in mind that the fatigue life range in which this extension is performed has to be consistent with the hypothesis of the fatigue strength criterion.

Typical uniaxial S–N curve models link the fatigue life to a stress parameter such as maximum stress or stress amplitude. The master curve concept aims to link the $\varpi_{g_{eq,dam}}$ parameter to the fatigue life. The advantage is here to use a unique set of parameters to describe this relation independently of the multiaxiality state or stress/strain temporal evolution. Let us assume a Basquin law type S–N curve so that:

$$\sigma_a(N) = \frac{C}{N^\gamma} \quad (35)$$

For the simple fully reversed tension case on smooth specimen we have:

$$\varpi_{g_{eq,dam}} = \frac{(\sigma_a)^2 - (\sigma^*)^2}{E} \quad (36)$$

So that finally the energy damage parameter–N curve equation is:

$$\varpi_{g_{eq,dam}}(N) = \frac{(C/N^\gamma)^2 - (\sigma^*)^2}{E} \quad (37)$$

Eq. (37) is supposed to be valid on any loading type while the identification of C and γ is performed with only one set of fatigue data on smooth specimens under uniaxial fully reversed loadings (tension–compression, rotating or plane bending) since the proposed non-local approach is able to take into account the effect, on the fatigue strength, of the stress/strain volumetric distribution.

For multiaxial variable amplitude loadings, if we consider a given load sequence S_1 of time length T_1 and a sequence S_p that consist in sequence S_1 repeated p times it is easy to show that:

$$\varpi_{g_{eq,dam},S_p} = p \varpi_{g_{eq,dam},S_1} \quad (38)$$

$$\lambda_{S_p} = p \lambda_{S_1} \quad (39)$$

so that

$$\frac{\varpi_{g_{eq,dam},S_p}}{\lambda_{S_p}} = \frac{\varpi_{g_{eq,dam},S_1}}{\lambda_{S_1}} \quad (40)$$

and

$$\lambda_p N_p = \lambda_1 N_1 \quad (41)$$

As a consequence, in order to obtain an energy damage parameter–N curve independent of p (more generally independent of the sequence length) we must not consider a $(\varpi_{g_{eq,dam}} - N)$ curve but a $(\varpi_{g_{eq,dam}} / \lambda - \lambda N)$ curve (see Fig. 4b).

Fig. 6 illustrates the results of the non-local approach on experimental data obtained on smooth specimens made of ER7 steel. Further analyses of the results presented in this figure will be

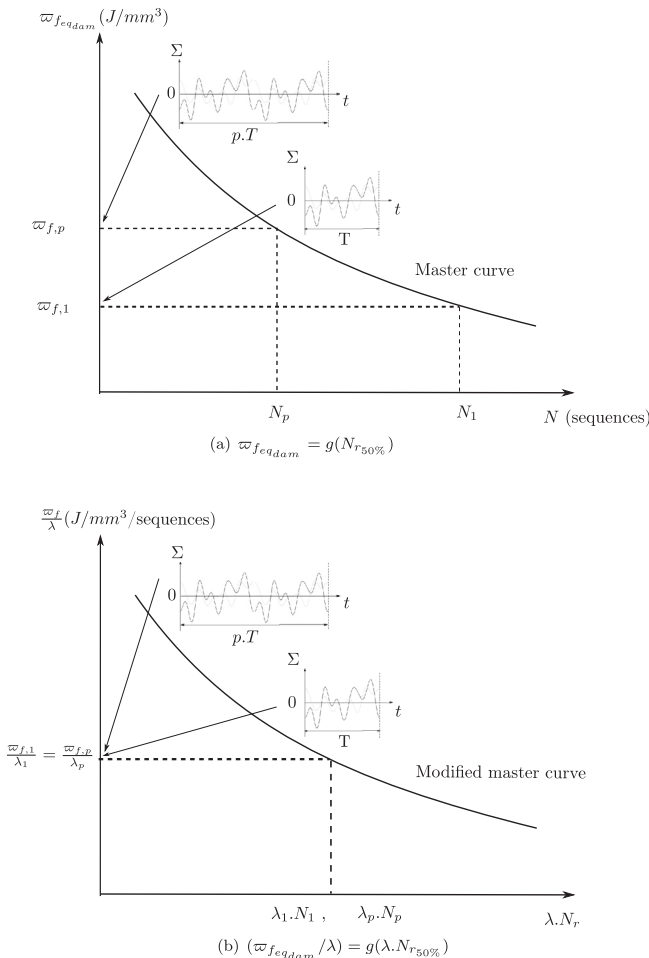


Fig. 4. (a) Usual and (b) Modified master curve representation.

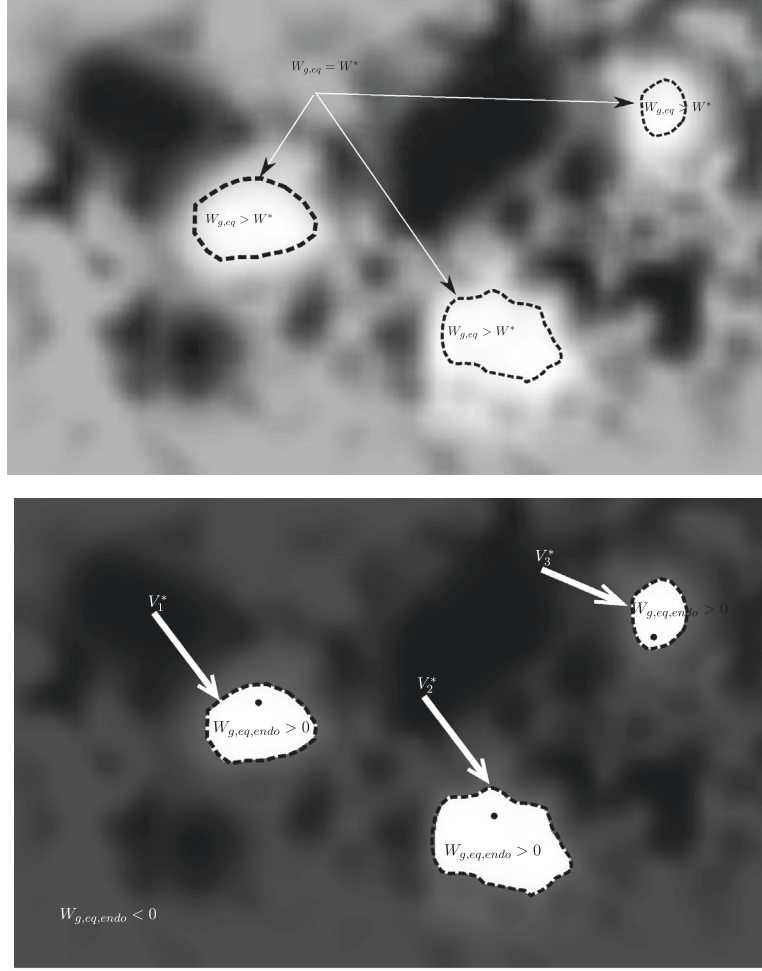


Fig. 5. Schematic 2D illustration of the damage parameter $W_{g,eq,dam}$. Critical points and illustration of the volumes influencing fatigue crack initiation.

proposed in the paper, but it is important to notice that from different S-N curves corresponding to different loading cases, a single $(\varpi_{g,eq,endo}/\lambda - \lambda N)$ curve is finally obtained. This approach unifies reasonably well all the experimental results.

3. Synoptic and how to apply the proposal

3.1. Identification of the parameters

Two material parameters (σ^* and β) have to be identified from 3 fatigue strengths in the high cycle fatigue regime (at 10^7 cycles for instance) on smooth specimens, under fully reversed loadings tension-compression $\sigma_{Ten,-1}^D$, rotating bending $\sigma_{RotBen,-1}^D$ and torsion $\sigma_{Tor,-1}^D$. The material parameter σ^* corresponds to the threshold stress amplitude, lower than the fatigue limit, below which no micro-crack initiates; it is identified according to Eq. (16). The endurance limit is seen as a threshold stress for non-propagating crack [18]. The β parameter, representative of the material sensitivity to the triaxiality of stresses, is the solution of Eq. (42) where ν is the Poisson ratio of the material (see Banvillet et al. [16] for more details). Furthermore one S-N curve on smooth specimens loaded under fully reversed uniaxial loading is needed to identify the master curve $\varpi_{g,eq,dam}(N)$ according to Eqs. (36) and (37).

$$\left(\frac{\sigma_{RotBen,-1}^D}{\sigma_{Tor,-1}^D}\right)^2 - 3 \left\{ 1 - \frac{1}{\beta} \ln \left[1 + \frac{1-2\nu}{3} (e^\beta - 1) \right] \right\} = 0 \quad (42)$$

3.2. Synoptic

The use of the proposed fatigue life assessment method on an industrial component requires a finite element analysis to compute W_g at all the points of the component from the stress and strain time history and to compute the volumetric average of W_g in the volume influencing fatigue crack initiation (V^*). Its application can be summarized as illustrated on the flow chart in Fig. 7.

4. Results

This section presents the comparison between experimental data and the assessment of the fatigue strength by the proposed approach. This section is organized in two parts: the first one is dedicated to the multiaxial fatigue strength criterion and the second one is dedicated to the fatigue life assessment method.

The considered materials are ER7 (ferritic-pearlitic steel), SAE1045, C35N and St35 steels and EN-GJS800-2 spheroidal graphite cast iron which mechanical properties are given in Table 1. Median values of the experimental fatigue strengths for all the investigated materials are given in Table 2. Results are presented separately for each loading type in the following sections. All the reported fatigue tests were carried out under load control.

4.1. Multiaxial fatigue strength criteria

The results of the proposal have been compared to three other well known high cycle multiaxial fatigue strength criteria:

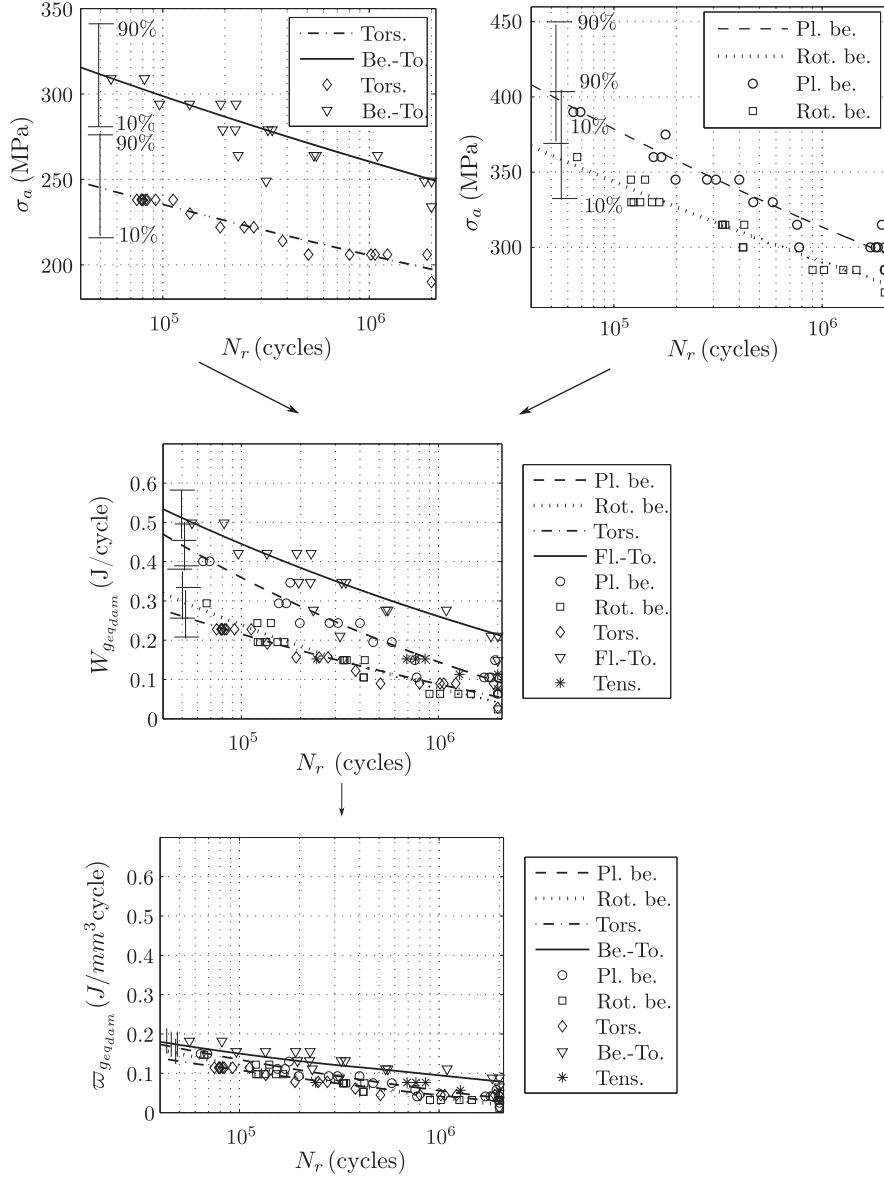


Fig. 6. $W_{g,eq,dam}$ and $w_{g,eq,dam}$ evolutions according to the median fatigue life for various loadings for ER7 steel.

Dang-Van et al. [25] (DV), Papadopoulos [26] (Pa) and Crossland [27] (Cr). These criteria are briefly presented in Appendix A. The quality of the high cycle multiaxial fatigue strength criteria has been evaluated by computing for different experimental load cases the classical safety coefficient C_s defined by:

$$C_s = \frac{\sigma_{threshold}}{\sigma_{eq}^D(exp)} \quad (43)$$

where $C_s > 1$ (resp. < 1) corresponds to a non-conservative (resp. conservative) prediction since the simulated fatigue strength is greater (resp. lower) than the experimental result. It has to be pointed out that in Eq. (43), $\sigma_{eq}^D(exp)$ is the equivalent stress of each criterion for the considered experimental fatigue data and $\sigma_{threshold}$ is the threshold of the criterion. Indeed, all the criterion can be written $\sigma_{eq}(M) \leq \sigma_{threshold}$ (see Appendix A).

Furthermore, since the proposed method is energy based, its damage variable, $w_{g,eq,dam}$, is proportional to a stress to the power 2. Consequently for having a safety coefficient proportional to a

stress ratio, like for the other criteria, the following ratio has been used when considering our proposal:

$$C_s = \sqrt{\frac{w_{g,eq,dam}^D}{w_{g,eq,dam}^D}} \quad (44)$$

Four types of loading were investigated: combined plane bending and torsion, combined rotative bending and torsion, combined tension and torsion, combined tension and torsion with internal pressure.

4.1.1. Results on ER7 steel

4.1.1.1. Non-proportional combined plane bending and torsion ($R_\sigma = R_\tau = -1$). Median experimental fatigue strengths at 2×10^6 cycles under non-proportional combined plane bending and torsion have been experimentally estimated on ER7 steel using the staircase method. Safety coefficients are given in Table 3. Like for Papadopoulos criterion, our proposal gives conservative results compared to other criteria: this is more secure for industrial applications.

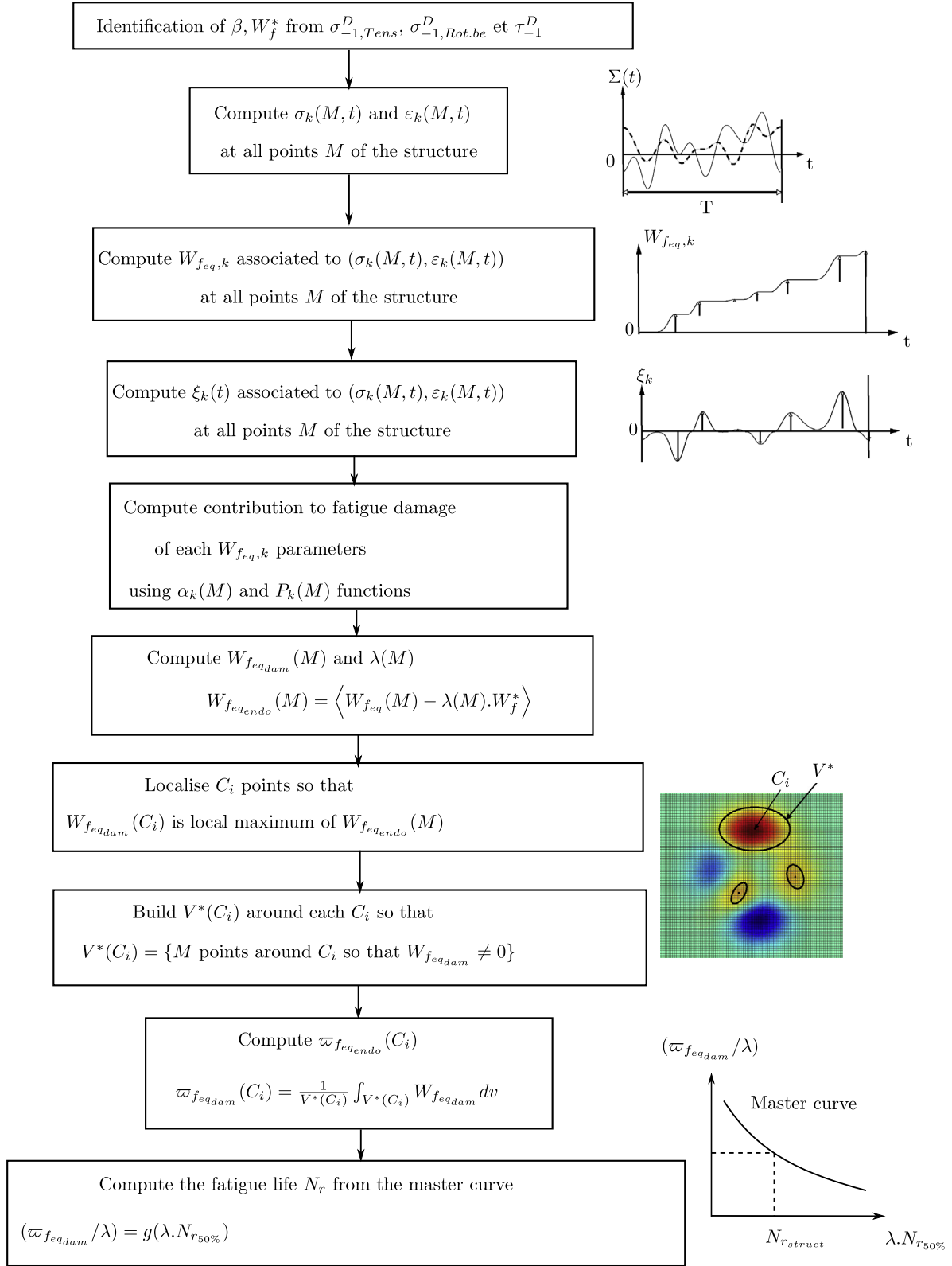


Fig. 7. Flow chart of the fatigue life assessment proposed method.

4.1.2. Results on SAE1045 steel

4.1.2.1. Combined proportional rotating bending and torsion. Safety coefficient distribution for combined proportional rotative bending and torsion results given by Gough and Pollard [28] for type SAE1045 steel are illustrated Fig. 8. The material parameters of the fatigue criteria were identified using the rotating bending

($R_\sigma = -1$) and torsion ($R_\tau = -1$) fatigue strengths given in the same paper [28].

For most of the cases, the proposal gives conservative results. It has to be noticed that in numerous cases, the maximum equivalent Von Mises stress exceed the yield stress of the material so that using a purely elastic behavior for computing the stress/strain

Table 1

Conventional yield stress at 0.2% plastic strain ($R_{p0.2}$) and tensile strength (R_m) of the tested materials under monotonic quasi-static tension.

Material	$R_{p0.2}$ (MPa)	R_m (MPa)	Reference
ER7	440	795	This study
SAE1045	–	624	[28]
C35N	313	550	[40]
St35	–	395	[29]
EN-GJS800-2	462	795	[13]

Table 2

Experimental fatigue strength at 10^6 cycles on smooth specimens under fully reversed ($R = -1$) tension ($\sigma_{Ten,-1}^D$), plane bending ($\sigma_{PB,-1}^D$) and rotative bending ($\sigma_{RotBen,-1}^D$) for all materials, except for ER7 steels for which the fatigue strengths are given at 2×10^6 cycles.

Material	$\sigma_{Ten,-1}^D$ (MPa)	$\sigma_{PB,-1}^D$ (MPa)	$\sigma_{RotBen,-1}^D$ (MPa)	$\sigma_{T0,-1}^D$ (MPa)	Reference
ER7	272	296	283	198	This study
SAE1045	–	584	560	371	[28]
C35N	–	205	190	150	[40]
St35	–	206	205	123	[29]
EN-GJS800-2	245	294	280	220	[13]

distribution may over-estimate the real distributions. For more accurate predictions, an elastoplastic computation should have been carried out but necessary mechanical properties were not available in the original paper. Dang Van criterion gives good results for these fatigue tests.

4.1.3. Results on St35 steel

4.1.3.1. Proportional combined tension and torsion with internal pressure. Richter et al. [29] have performed proportional combined tension–torsion and internal pressure on St35 steel smooth specimens at 10^6 cycles. Fig. 9 illustrates the distribution of safety coefficients for that particular loading case. Except for Crossland criterion that gives strongly non-conservative results, other criteria give reasonably good results with safety coefficients in the range $[-0.8; +1.2]$. Once again, our approach shows a conservative trend.

Table 3

Median experimental fatigue strengths at 2×10^6 cycles on smooth type ER7 steel specimens under combined plane bending and torsion with a phase shift φ and corresponding safety coefficients of the tested criteria (Pro = proposal, DV = Dang Van, Pa = Papadopoulos, Cr = Crossland).

σ_a (MPa)	τ_a (MPa)	φ	C_s Pro	C_s DV	C_s Pa	C_s Cr
257	153	$\pi/2$	0.92	1.14	0.83	1.1

4.1.4. Conclusions about the proposed non-local high cycle multiaxial fatigue strength criterion

The simulated fatigue strengths with the proposal are in good agreement with a large set of experimental data under proportional and non-proportional loadings. Most of the time these previsions are conservative whereas the previsions of the other tested criteria are non-conservative and may lead to dangerous results in design departments. The proposal is able to take into account the following effects on the fatigue strength: the loading type (tension, rotating bending, plane bending) and the volumetric stress–strain distribution in the components.

Furthermore, for the local criteria which do not distinguish the load type effect, their previsions may be large when the uniaxial fatigue strength used for identifying the material parameters is chosen between the following possible experimental values: tension or rotating bending or plane bending.

4.2. Fatigue life assessment method

Three data set obtained on three different materials are used in the following to evaluate the proposed fatigue life assessment method: EN-GJS800-2 spheroidal graphite (SG) cast iron [11,13,30], 10HNAP steel [31–34] and an ER7 steel (this study). For all these experiments the fatigue tests were carried out up to the detection of a technical fatigue crack (typical length of 1 mm); the macroscopic fatigue crack growth is not considered.

4.2.1. EN-GJS800-2 SG cast iron results [30,13,11]

Computed fatigue life were obtained considering the S–N curve under fully reversed plane bending loading ($R_\sigma = -1$) as the master curve modeled using a Basquin type equation without asymptote. For the EN-GJS800-2 SG cast iron, the threshold stress σ^* is 210 MPa and $\beta = 3.1$.

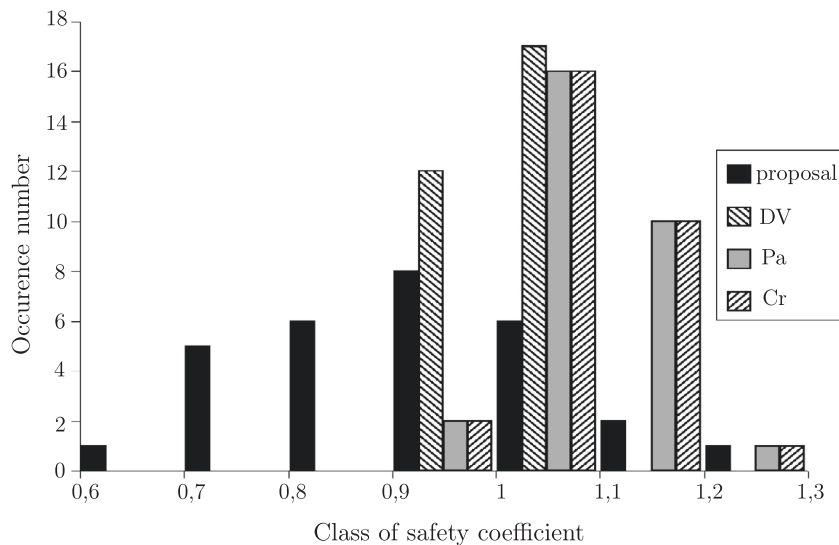


Fig. 8. Safety coefficients distributions for the constant amplitude fatigue tests under combined rotative bending and torsion on smooth SAE1045 specimens (DV = DangVan, Pa = Papadopoulos, Cr = Crossland) [28].

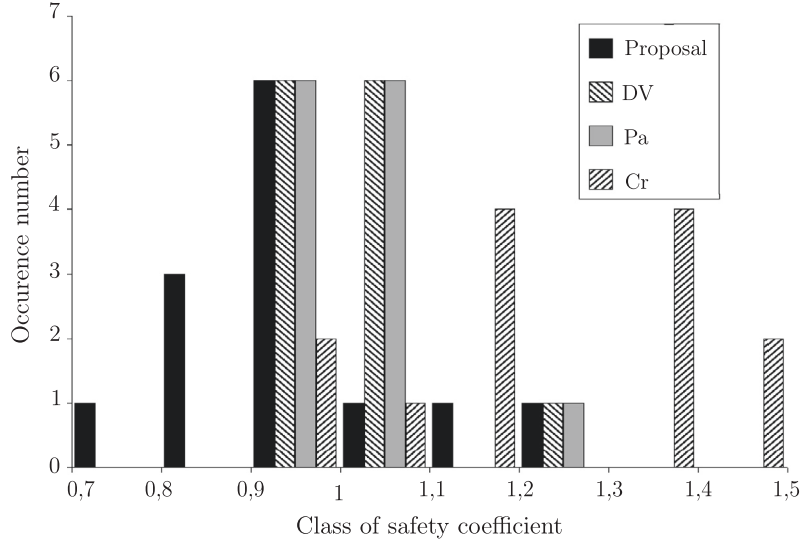


Fig. 9. Comparison of the safety coefficients for the constant amplitude fatigue tests under the combined tension and torsion with internal pressure on smooth specimens of St35 steel (DV = DangVan, Pa = Papadopoulos, Cr = Crossland) [29].

4.2.1.1. Combined fully reversed plane bending and torsion ($R_\sigma = R_\tau = -1$) at different frequencies. Testing conditions are given in Table 4, where f_σ/f_τ represent the frequency ratio. The plane bending frequency is kept to $f_\sigma = 50$ Hz. It is important to notice that such tests induce non-proportional multiaxial stress states. For each test series 10 specimens are tested. Table 4 summarizes the loading conditions, the experimental results (N_{exp}), in terms of median values, and simulated ones (N_{sim}) by the proposal. Experimental results are given in terms of load sequence number to failure, one sequence including only one torsion cycle (torsion is the lower frequency loading when two frequencies are applied).

4.2.1.2. High/low block loadings under fully reversed plane bending or torsion. The test sequences consist of two blocks of fully reversed torsion ($R_\tau = -1$) (respectively of plane bending ($R_\sigma = -1$)) with two different stress amplitude $\Delta\sigma_1/2$ and $\Delta\sigma_2/2$ and of equal length (5000 cycles). These two blocks are alternatively applied on the specimen until macroscopic crack initiation.

Experimental loading conditions, number of sequences to macroscopic crack initiation and simulated number of sequences to failure are given in Tables 5 and 6.

4.2.1.3. Variable amplitude loadings of simple plane bending or combined plane-bending and torsion. Experimental results obtained in [11] using in service recorded variable amplitude loadings representative of stress/strain on automotive suspension arm have been used to evaluate the quality of the fatigue life simulation under real variable amplitude load sequence. Signal levels were chosen so that, if a Rainflow analyses is performed, the extracted maximum stress amplitude corresponds to a fatigue life of 10^5 cycles. Sequences are reproduced until technical crack initiation (typical length, depth of 1 mm). Three series of tests were performed: simple bending, torsion and combined bending and torsion.

For constant amplitude loadings, the phase shift quantifies the desynchronism between two cyclic loadings. For variable amplitude loadings the desynchronism can be described by an estimator ρ_{xy} of the correlation coefficient noted r_{xy} . Let us consider X and Y two continuous random variables. The correlation coefficient r_{XY} is defined as follows:

$$r_{XY} = \frac{cov(X, Y)}{S_X S_Y} \quad (45)$$

Table 4

Different frequencies experimental loading conditions, test results (N_{exp}) and simulated fatigue life with the proposal (N_{sim}).

σ_a (MPa)	τ_a (MPa)	f_σ/f_τ	N_{exp} (sequences)	N_{sim} (sequences)
225	167	1	122,191	235,000
225	167	5	9893	7513
155	204	1	119,911	106,000
155	204	5	17,357	13,047

where $cov(X, Y)$ is the covariance and S_X (resp. S_Y), the standard deviation of X (resp. Y) [35]. For discrete variables x and y , an estimator ρ_{xy} of the correlation coefficient is given by the following equation where n is the size (number of values) of the samples x and y ; \bar{x} and \bar{y} are the mean value estimators ($\bar{x} = \frac{1}{N} \sum_{i=1}^N x_i$).

$$\rho_{xy} = \frac{\sum_{i=1}^n (x_i - \bar{x})(y_i - \bar{y})}{\sqrt{\sum_{i=1}^n (x_i - \bar{x})^2 \sum_{i=1}^n (y_i - \bar{y})^2}} \quad (46)$$

In any cases ρ_{xy} is in the following interval: $-1 \leq \rho_{xy} \leq 1$. If $\rho_{xy} = 0$ signals are not correlated (extrema do not occur at the same time). When $\rho_{xy} = 1$ signals are homotetic and synchronous, the load path is proportional. When $\rho_{xy} = -1$ signals are in phase opposition.

Experimental loading conditions including the correlation coefficient, experimental and simulated fatigue lives are presented

Table 5

Loadings with two blocks of plane bending ($R_\sigma = -1$) alternatively applied (low/high/low/...): experimental loading conditions, test results (N_{exp}) and simulated fatigue life with the proposal (N_{sim}) [13,30].

Loading	$\Delta\sigma_1/2$ (MPa)	$\Delta\sigma_2/2$ (MPa)	N_{exp} (cycles)	N_{sim} (cycles)
Pl. Bending	230	317	452,898	318,512
Pl. Bending	317	347	154,921	127,346
Pl. Bending	260	317	479,192	396,718
Pl. Bending	230	317	451,305	408,549
Pl. Bending	140	317	458,606	368,217
Pl. Bending	140	347	223,357	179,673
Pl. Bending	230	347	245,980	210,218
Pl. Bending	260	347	220,675	185,856
Pl. Bending	280	347	194,421	251,578
Pl. Bending	70	347	253,000	324,521

Table 6

Loadings with two blocks of torsion ($R_\tau = -1$) alternatively applied: experimental loading conditions, test results (N_{exp}) and simulated fatigue life with the proposal (N_{sim}) [11].

Loading	$\Delta\tau_1/2$ (MPa)	$\Delta\tau_2/2$ (MPa)	N_{exp} (cycles)	N_{sim} (cycles)
Torsion	250	100	291,645	346,217
Torsion	250	130	266,450	318,491
Torsion	250	180	266,451	271,359
Torsion	250	200	227,396	248,873
Torsion	250	230	168,153	201,392

Table 8

Loading conditions, simulated and median experimental fatigue lives (in seconds) for uniaxial variable amplitude loadings on 10HNAP flat smooth specimens [32].

σ_{max} (MPa)	σ_{min} (MPa)	$\bar{\sigma}$ (MPa)	T_{exp} (s)	T_{sim} (s)
292	-302	-7	111,954	85,249
312	-310	-1	90,839	53,227
320	-325	-13	70,325	45,203
343	-33	11	47,937	38,432
351	-349	-6	34,109	32,858
362	-360	7	23,364	27,649
370	-384	-13	18,051	22,675
386	-380	1	16,976	21,984
399	-398	-3	10,629	18,310

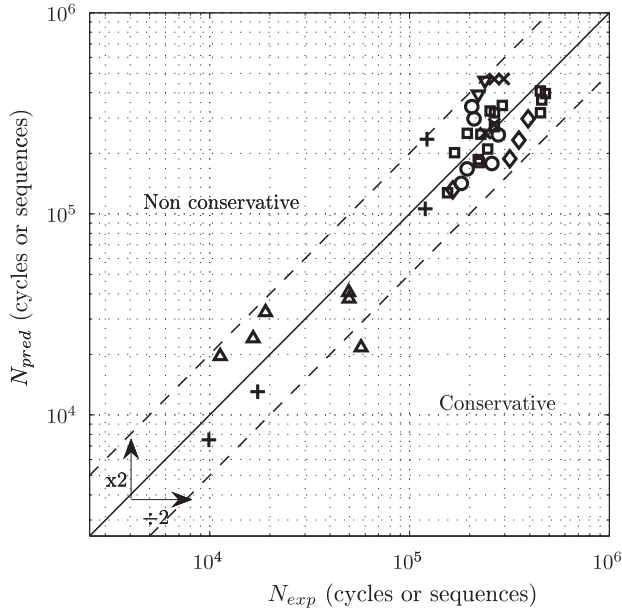
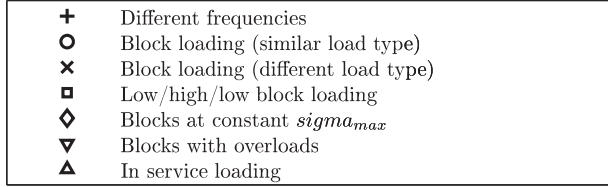


Fig. 10. Experimental and simulated fatigue lives (for in service loadings fatigue life is expressed in number of load sequences) for different loading cases on EN-GJS800-2 smooth specimens.

Table 7. The correlation coefficient $\rho_{\sigma\tau}$ is indicated. The loading path of test number 6 (Table 7) is quasi proportional. For test number 3, plane bending and torsion loadings are fully decorrelated, the load path is strongly non-proportional).

4.2.1.4. Discussion. Fig. 10 compares experimental and predicted fatigue life for above cited complex loadings on EN-GJS800-2 SG cast iron. In all cases the proposal gives satisfactory results, almost all the computed fatigue lives being in the scatter band of factor 2

Table 7

Loading conditions, simulated and experimental fatigue lives for variable amplitude loading on smooth specimens, EN-GJS800-2 SG cast iron from [11].

No.	Loading	σ_{max} (MPa)	τ_{max} (MPa)	σ_{min} (MPa)	τ_{min} (MPa)	$\rho_{\sigma\tau}$	N_{exp} (seq.)	N_{sim} (seq.)
1	Tor.	0	254	0	-231	-	19,020	32,403
2	Fl. Pl.	363	0	-313	0	-	11,268	19,617
3	Fl.pl. + Tor.	240	186	-248	-172	0.04	9587	21,658
4	Fl.pl. + T.	240	186	-248	-172	0.62	57,174	24,031
5	Fl.pl. + Tor.	225	167	-188	-147	0.51	16,496	37,862
6	Fl.pl.+ Tor.	225	167	-233	-147	0.94	49,760	40,828

Table 9

Loading conditions, simulated and median experimental fatigue lives (in seconds) for biaxial variable amplitude loadings on 10HNAP cross shaped specimens.

T_{exp} (s)	T_{sim} (s)
1,165,700	2,245,639
70,500	58,227
58,800	31,530
102,200	267,390
188,000	289,536
141,800	112,063
309,600	138,277
298,800	174,923
462,200	256,028

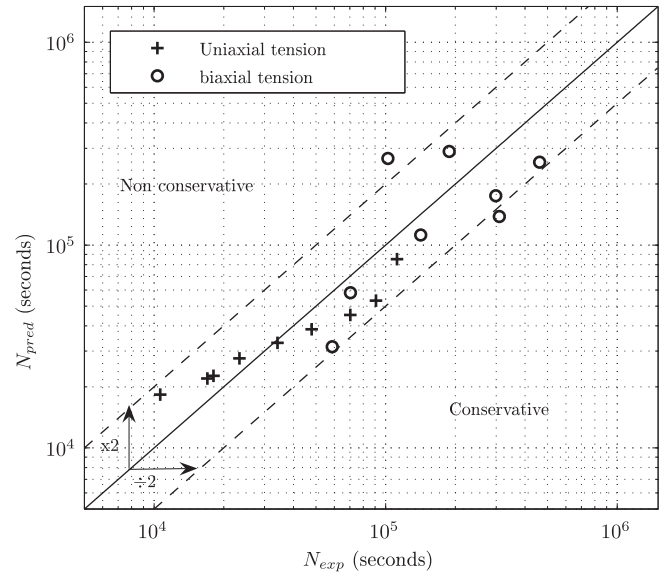


Fig. 11. Comparison of experimental and simulated fatigue lives for uniaxial and biaxial variable amplitude fatigue tests on 10HNAP steel.

$[N_{exp}/2; 2N_{exp}]$. However, our proposal does not give systematically conservative results like that was the case for constant amplitude

Table 10

Quasi-static mechanical characteristics under monotonic tension and experimental median fatigue strengths at 2×10^6 cycles on cylindrical smooth specimens of ER7 steel.

E (GPa)	ν (-)	$R_{e0.2}$ (MPa)	R_m (MPa)	$\sigma_{P_{-1}}^D$ (MPa)	$\sigma_{P_{B,-1}}^D$ (MPa)	$\sigma_{R_{B,-1}}^D$ (MPa)	τ_{-1}^D (MPa)
210	0.29	440	795	272	296	283	198

Table 11

Test conditions, experimental median fatigue lives and simulations for the combined plane bending and torsion tests ($R_\sigma = -1$) with different frequencies on ER7 steel, where $k_\sigma = \frac{\sigma_a}{\tau_a}$.

σ_a (MPa)	τ_a (MPa)	f_σ/f_τ	k_σ	N_{exp} (sequences)	N_{sim} (sequences)
294	182	8	1.61	11,036	10,598
294	182	1/8	1.61	10,695	15,702
135	218	8	0.61	34,793	18,211
135	218	1/8	0.61	11,529	17,436

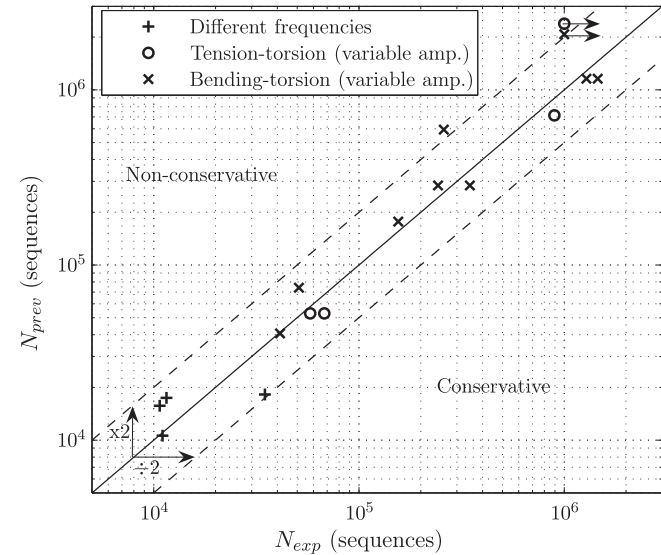


Fig. 12. Comparison of experimental and simulated fatigue lives with fatigue life calculation method on different fatigue tests on ER7 steel smooth specimens.

Table 12

Simulations and experimental median fatigue lives under variable amplitude combined bending and torsion loadings on smooth specimens of the ER7 steel, where $k_\sigma = \frac{\sigma_{max}}{\tau_{max}}$.

σ_{max}	τ_{max}	k_σ	$N_{exp50\%}$	N_{sim}	Comments
102	25	1	-	-	No cracks at 2×10^6 sequences
359	86	4	-	2,074,376	No cracks at 2×10^6 sequences
402	96	4.5	1,454,800	1,157,201	
402	96	4.5	1,282,600	1,157,201	
415	99	4.65	258,950	592,417	
424	102	4.75	346,750	284,366	
424	102	4.75	242,500	284,366	
445	107	5	155,350	177,053	
488	117	5.5	50,950	74,194	
531	127	6	41,250	40,698	

Table 13

Simulations and experimental median fatigue lives under variable amplitude combined tension and torsion loadings on smooth specimens of the ER7 steel where $k_\sigma = \frac{\sigma_{max}}{\tau_{max}}$.

σ_{max}	τ_{max}	k_σ	$N_{r50\%}$	N_{sim}	Comments
224	54	2.5	-	2,384,258	No cracks at 2×10^6 sequences
359	86	4	894,766	715,276	
445	107	5	57,843	52,935	
445	107	5	67,731	52,935	

loadings. But it has to be pointed out that the proposal is cycle counting technique independent. This is a significant advantage because several techniques exist in literature (level crossing, range pairs, rainflow, etc.) but none for non-proportional loadings [10]. Under non-proportional loadings a cycle counting variable has to be defined, but many fatigue life calculation methods need to count on a variable which is not the damage variable and that may lead to omit some damaging part of the loading.

4.2.2. Uniaxial and biaxial variable amplitude loadings on 10HNAP steel

Fatigue test results on 10HNAP steel were obtained from [31–34]. The reference master curve that is considered here is the plane bending S-N curve ($R_\sigma = -1$) modeled using the Basquin type equation. For this material $\sigma^* = 207$ MPa and $\beta = 2.4$.

4.2.2.1. Uniaxial variable amplitude tensile loading.

Fatigue tests were performed on flat smooth specimens. The loading sequence

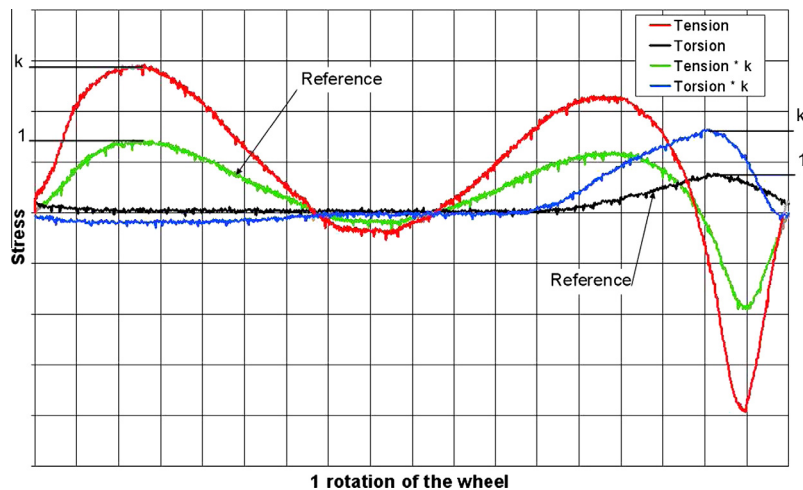


Fig. 13. Variable amplitude combined tension and torsion load history and illustration of the magnification factor k .



Fig. 14. Drilled wheel on SNCF-AEF fatigue test bench.

Table 14

Experimental and predicted fatigue lives on a railway wheel for constant amplitude and block-program sequence.

	N_{exp} (cycles or sequences)	N_{pred} (cycles or sequences)	Comments
CA Test 1	980,000	845,934	
CA Test 2	225,000	178,376	
Block Test No. 1	10,625	12,500	
Block Test No. 2	>12,500	31,250	No cracks at 12,500 sequences

consists of a 649 s, large spectral band width (0–40 Hz) and stationary signal. For each test series four specimens were tested, the loading level being increased (scaled up) for each series so that different life range could be investigated. Loading conditions, experimental and computed fatigue lives are given in Table 8.

4.2.2.2. *Biaxial variable amplitude tensile tests on cross shaped specimens.* For these tests the loading signals are stationary, ergodic with normal distributions centred on a zero mean stress [31]. The correlation coefficient of the two signals is close to -1 (ranging from -0.95 to -0.99) so that they can be considered as uncorrelated out of phase signals. Table 9 presents experimental and simulated fatigue lives in terms of time to failure (i.e. technical fatigue crack initiation).

4.2.2.3. *Discussion.* Comparison of simulated and experimental fatigue lives are presented in Fig. 11. In all cases, the predictions of the

proposal are in good agreement with the experimental results. For shorter fatigue life range the predictions of the proposal tend to be less conservative but still lies within the ratio of two scatter band delimited by the two dashed lines.

4.3. ER7 steel

The various characteristics of the ER7 steel (close to SAE1045 steel) are given in Table 10. The reference S–N curve is identified from fully reversed plane bending results on smooth specimens using a Basquin model. For this steel, the threshold stress σ^* is equal to 258 MPa and the material parameter β is 2.

4.3.1. Combined plane bending and torsion tests ($R_\sigma = -1$) with different frequencies

Comparison between experimental and computed fatigue life for fully reversed combined plane bending and torsion results are presented in Table 11, where f_σ/f_τ indicates the frequency ratio between the bending and torsion stresses (the bending stress frequency, f_σ is 48 Hz). Ten specimens were tested for each tests series.

4.3.2. Variable amplitude stresses specific to the railway field

A typical non-proportional multiaxial loading (see Fig. 13) encountered on railway wheels has been applied on smooth specimens under combined tension torsion at the LFM (University of Metz) and combined bending torsion at the LAMEFIP (Arts et Métiers ParisTech, Bordeaux Center). The reference signal amplitude was magnified by a factor k in order to obtain experimental fatigue lives in the range 10^4 – 2×10^6 cycles. All the results are given in Tables 12 and 13.

4.3.2.1. *Discussion.* Fig. 12 shows that the predictions of the proposed fatigue life calculation method remain in an interval of more or less two times the experimental fatigue life. These assessments are good for non-proportional loadings. The proposed method gives good assessments for tests known as discriminating (non-proportional loadings: combined loadings with different frequencies). We can also note that the predictions are good for variable amplitude loading with a relatively low number of cycles to fatigue crack initiation (medium cycle fatigue). The interest of such an energy based calculation method is its fast computation time compared with a critical plane approach for which looking for the critical plane is time consuming. Moreover, finding an appropriate method for identifying a critical plane under variable amplitude non-proportional loading is still an open problem.

4.3.3. Test of a real railway wheel (full scale)

Uniaxial fatigue tests under constant amplitude and block-program sequence were carried out by SNCF-AEF on a railway wheel (in ER7 steel). Two holes (Fig. 14) were machined on the wheel

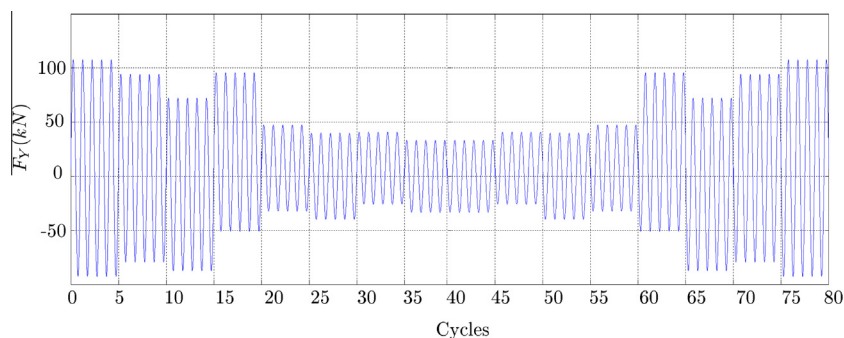


Fig. 15. Loadings applied for the first tests with blocks.

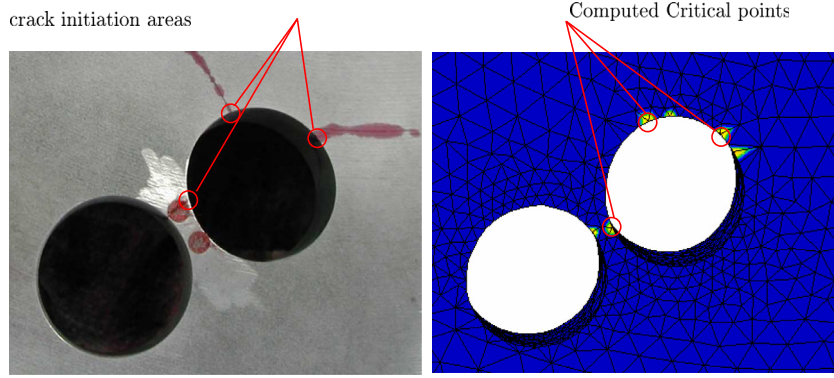


Fig. 16. Comparison between the experimental fatigue crack initiation sites and the critical points computed by the proposed method.

to create a local multiaxial stress state and to better evaluate the accuracy of the proposed non-local fatigue life calculation method. The wheel was tested on the SNCF-AEF fatigue test bench under a lateral load F_y (parallel to the wheel axis, see Fig. 14). Two constant amplitude loading tests were performed at 10 Hz at a loading level of $F_y = \pm 80$ kN and $F_y = \pm 120$ kN respectively referenced as CA Test 1 and CA Test 2 in Table 14. The typical block type loading illustrated Fig. 15 was established from in service strain measurement recordings by using the block-program technique [36] and a mean load correction with an Haigh diagram. Due to the low frequency of the fatigue test (1.6 Hz) only two block-program tests could be performed (referenced as Block Test 1 and Block Test 2 in Table 14). The second test was stopped before crack initiation after 12,500 load sequences.

The experimental and simulated number of sequences up to technical fatigue crack initiation (monitored with a strain gauge glued between the two holes) are given in Table 14 and show a good agreement between experimental and simulated fatigue lifes. For the fourth test, no crack was observed after 12,500 sequences as computed by the proposal.

Fig. 16 illustrates the good correlation between experimental and computed fatigue crack initiation location.

5. Conclusion and prospects

The high cycle multiaxial fatigue criterion and its extension to a fatigue life assessment method proposed in this paper was found to give good results for both proportional and non-proportional multiaxial variable amplitude loadings on various metallic materials. This is true even under discriminating loading conditions on specimens so that (i) out-of-phase loadings, (ii) combined loadings with different frequencies, and (iii) variable amplitude loading sequence under combined loadings from in service measurement. The methodology was successfully applied to a real industrial case submitted to variable amplitude loading too.

The following remarks can be made:

- In order to identify the material parameters (W^* , β) of the proposal three fatigue strengths under fully reversed loadings have to be experimentally determined on smooth specimens: tension, torsion and rotating bending. For the fatigue life assessment method, an additional S–N curve is needed (no particular loading type is required here) to identify the master curve relating the damage parameter and the fatigue life.
- The phase shift effect experimentally observed under biaxial tension is well reproduced: fatigue strength of brittle (resp. ductile) materials increase (resp. decrease) with the phase shift. The fatigue strength in the HCF regime is not sensitive to the

phase shift between tension (or bending) and torsion (this was not detailed in this paper but this quality is an heritage of the previous formulation [16]).

- The methodology was successfully implemented as a finite element post-processor that makes it possible to apply to any industrial structure submitted to constant or variable amplitude multiaxial loadings.
- Being a non-local approach, the proposal makes it possible to consider gradient effects in specimens or structures. For example it is possible to differentiate tensile and plane bending fatigue strengths even if the local stress/strain state are similar. Notch effects and more generally stress/strain gradients effects on structures can be taken into account. It is particularly interesting for structures where usual methods to take stress/strain gradients into account [4,37] fails under non-proportional variable amplitude loadings (usually the gradient direction has to be defined in the cited methods which is not the case with our proposal).

Some improvement and further validations have still to be made to the proposal. In particular W_f^* does not depend on the mean stress level. This point should be experimentally validated. In addition, the approach needs to be further validated on notched specimens on a large variety of materials. Some data are available in the literature however they generally suffer of sufficient details on the cyclic behavior of the tested materials. Good knowledge of elastoplastic cyclic behavior are necessary to correctly describe the stress/strain fields in the notched areas in particular under multiaxial variable amplitude loadings. Furthermore, additional work has to be done for considering the positive effect of compressive normal stress on the fatigue strength and life. In the proposal there is no difference between tensile and compressive mean normal stress, however the simulations are conservative when compressive mean stress occurs.

Appendix A. Brief presentation of the tested high cycle multiaxial fatigue criteria

The Crossland criterion [38] is defined by a linear relationship between the maximum, on the loading period T , of the hydrostatic stress $\Sigma_{H,max}$ and the amplitude τ_{aJ_2} of $\sqrt{J_2(t)}$, where $J_2(t)$ is the second invariant of the deviatoric stress tensor (47):

$$\tau_{aJ_2}(M) = \frac{1}{2\sqrt{2}} \max_{t \in T} \left\{ \max_{t' \in T} \left[\sqrt{(\underline{\underline{S}}(M,t) - \underline{\underline{S}}(M,t')) : (\underline{\underline{S}}(M,t) - \underline{\underline{S}}(M,t'))} \right] \right\}$$

The Crossland criterion is given in the following equation:

$$\sigma_{eq,Cr}(M) = \tau_{aJ_2}(M) + a \Sigma_{H,max}(M) \leq b \quad (47)$$

The material parameters a and b are given by the following equations: $a = (3\sigma_{Tors,-1}^D / \sigma_{uniax,-1}^D) - \sqrt{3}$ and $b = \sigma_{Tors,-1}^D$, where $\sigma_{uniax,-1}^D$ is the fully reversed endurance limit for a uniaxial stress state (tension, plane bending or rotating bending) and σ_{-1}^D is the endurance limit in fully reversed torsion, on smooth specimens.

The Dang-Van model is a critical plane criterion based on a mesoscopic–macroscopic scale change [25]. It can be expressed as Eq. (48) where $\|\vec{\tau}_a(M, \vec{n}, t)\|$ is the amplitude of the shear stress vector acting on the material plane orientated by the unit normal vector \vec{n} at the point $M, \Sigma_H(M)$ is the hydrostatic stress. The parameters c and d are identified from two experimental endurance limits on smooth specimens, for instance: $c = (3\sigma_{Tors,-1}^D / \sigma_{uniax,-1}^D) - (3/2)$ and $d = \sigma_{Tors,-1}^D$.

$$\sigma_{eq,DV}(M) = \max_{\vec{n}} \left\{ \max_{t \in T} \left[\|\vec{\tau}_a(M, \vec{n}, t)\| + c\Sigma_H(M, t) \right] \right\} \leq d \quad (48)$$

Depending on the value of the ratio $\sigma_{Tors,-1}^D / \sigma_{Ten,-1}^D$ of the material, Papadopoulos [26,39] proposed two high cycle multiaxial fatigue criteria based on a mesoscopic approach. These criteria are built with two root mean square quantities. The first one, noted T_σ (49), is related to the macroscopic resolved shear stress amplitude T_a acting on all the possible directions (located by the angle ψ) of a material plane (orientated by the unit normal vector \vec{n} , defined by the angles θ and ϕ). The second, noted M_σ , is the root mean square value of T_σ on all the possible material planes (50); it is called “an integral approach”.

$$T_\sigma(M, \theta, \phi) = \sqrt{\frac{1}{\pi} \int_{\psi=0}^{2\pi} T_a^2(\theta, \phi, \psi) d\psi} \quad (49)$$

$$M_\sigma(M) = \sqrt{\frac{5}{8\pi^2} \int_{\phi=0}^{\phi=2\pi} \int_{\theta=0}^{\theta=\pi} T_\sigma^2(\theta, \phi) \sin \theta d\theta d\phi} \quad (50)$$

Finally, the two endurance criteria are defined by Eqs. (51) and (52). The material parameters are related to two fully reversed endurance limits on smooth specimens in torsion $\sigma_{Tors,-1}^D$ and in uniaxial stress state $\sigma_{uniax,-1}^D$ (tension, plane or rotating bending): $e = (3\sigma_{Tors,-1}^D / \sigma_{uniax,-1}^D) - (3/2)$, $f = \sigma_{Tors,-1}^D$ and $g = (3\sigma_{Tors,-1}^D / \sigma_{uniax,-1}^D) - \sqrt{3}$, $h = \sigma_{Tors,-1}^D$. In this paper the T_σ approach has been considered only.

$$\text{If } 0.5 \leq \tau_{-1}^D / \sigma_{Ten,-1}^D \leq 0.6, \quad \sigma_{eq,Pa,T\sigma}(M) \\ = \max_{\theta, \phi} [T_\sigma(M, \theta, \phi)] + e\Sigma_{H,max}(M) \leq f \quad (51)$$

$$\text{If } 0.6 \leq \tau_{-1}^D / \sigma_{Ten,-1}^D \leq 0.8, \quad \sigma_{eq,Pa,M\sigma}(M) \\ = M_\sigma(M) + g\Sigma_{H,max}(M) \leq h \quad (52)$$

References

- [1] Berger C, Eulitz K-G, Heuler P, Kotte K-L, Naundorf H, Schuetz W, et al. Betriebsfestigkeit in Germany – an overview. *Int J Fatigue* 2002;24:603–25.
- [2] Palin-Luc T, Lasserre S. An energy based criterion for high cycle multiaxial fatigue. *Eur J Mech A/Solids* 1998;17(2):237–51.
- [3] Sonsino CM, Kaufmann H, Grubisic V. Transferability of material data for the example of a randomly loaded forged truck stub axle. In: SAE International, editor. SAE Tech. Paper series, number 970708 in SAE technical paper, Detroit. SAE; February 1997. p. 1–22.
- [4] Qylafku G, Azari Z, Kadi N, Gjonaj M, Pluvinage G. Application of a new model proposal for fatigue life prediction on notches and key-seats. *Int J Fatigue* 1999;21:753–60.
- [5] Schijve J. Fatigue of structures and materials in the 20th century and the state of the art. *Int J Fatigue* 2003;23(8):679–702.
- [6] Jasper TM. The value of the energy relation in the testing of ferrous metals at varying ranges and at intermediate and high temperature. *Philos Mag* 1923;46(274):609–27.
- [7] Ellyin F. Cyclic strain energy density as a criterion for multiaxial fatigue failure. In: Brown, Miller, editors. *Biaxial and multiaxial fatigue*, vol. 3. London: EGF Publication; 1989. p. 571–83.
- [8] Ellyin F. *Fatigue damage, crack growth and life prediction*. Edmonton, Canada: Chapman and Hall; 1997. 469p.
- [9] Macha E, Sonsino CM. Energy criteria of multiaxial fatigue failure. *Fatigue Fract Eng Mater Struct* 1999;22:1053–70.
- [10] Palin-Luc T. Fatigue under variable amplitude loadings. In: Bathias Claude et Pineau André, editor. *Fatigue of materials and structures, fundamentals*. ISTE and Wiley publishers; 2010. p. 457–502 [Chapter 12]. ISBN 978-1-84821-0516.
- [11] Banvillet A. Prévission de la durée de vie en fatigue multiaxiale sous spectre de chargement réel: vers des essais accélérés. PhD thesis, ENSAM CER de Bordeaux; 2001.
- [12] Banvillet A, Lagoda T, Macha E, Nieslony A, Palin-Luc T, Vittori J-F. Fatigue life under non gaussian random loading from various models. *Int J Fatigue* 2004;349–63.
- [13] Palin-Luc T. Fatigue multiaxiale d'une fonte GS sous sollicitations combinées d'amplitude variable. PhD thesis, ENSAM CER de Bordeaux, France; 1996. 261p.
- [14] Froustey C, Lasserre S, Dubar L. Essais de fatigue multiaxiaux et par blocs. Validité d'un critère pour les matériaux métalliques. *Mat-Tech* 92. IITT-International; 1992. p. 79–85.
- [15] Lemaître J, Chaboche J-L. *Mécanique des matériaux solides*. Paris: Dunod; 1988. 544p.
- [16] Banvillet A, Palin-Luc T, Lasserre S. A volumetric energy based high cycle multiaxial fatigue criterion. *Int J Fatigue* 2003;26(8):755–69.
- [17] Froustey C, Lasserre S. Multiaxial fatigue endurance of 30NCD16 steel. *Int J Fatigue* 1989;11(3):169–75.
- [18] Palin-Luc T, Lasserre S, Bérard J-Y. Experimental investigation on the significance of the conventional endurance limit of a spheroidal graphite cast iron. *Fatigue Fract Eng Mater Struct* 1998;21(3):192–200.
- [19] Bathias C, Paris PC. *Gigacycle fatigue in mechanical practice*. Marcel Dekker; 2005.
- [20] Banvillet A, Palin-Luc T, Lasserre S. A volumetric energy based high cycle multiaxial fatigue criterion. *Int J Fatigue* 2003;25:755–69.
- [21] Hyde TH. The uniaxial and biaxial, monotonic and cyclic plasticity behaviour of a lead alloy model material. *J Strain Anal* 1993;18:125–33.
- [22] Lagoda T. Energy models for fatigue life estimation under uniaxial random loading. Part I: The model elaboration. *Int J Fatigue* 2001;23:467–81.
- [23] Lagoda T. Energy models for fatigue life estimation under uniaxial random loading. Part II: Verification of the model. *Int J Fatigue* 2001;23:481–9.
- [24] Weber B, Carmet A, Kenneugne B, Robert JL. On a global stress based approach for fatigue assessment under multiaxial random loading. *Eng Against Fatigue* 1999;407–14.
- [25] Dang-Van K, Cailletaud G, Flavenot J-F, Douaron Le, Lieurade H-P. Criterion for high-cycle fatigue failure under multiaxial loading. In: Brown MW, Miller KJ, editors. *Biaxial and multiaxial fatigue*. Sheffield; 1989. p. 459–78.
- [26] Papadopoulos IV. A new criterion of fatigue strength for out-of-phase bending and torsion of hard metals. *Int J Fatigue* 1994;16(6):377–84.
- [27] Crossland B. Effect of a large hydrostatic pressure on the torsional fatigue strength of an alloy steel. In: *Int conf fatigue of metals*. London: Inst. of Mech. Eng.; 1959a. p. 138–149.
- [28] Gough HJ, Pollard HV. The strength of metals under combined alternating stresses. In: *Proceedings of the institution of mechanical engineers*, vol. 131. London; November 1935. p. 1–103.
- [29] Richter I, Zenner H, Heidenreich R. Bewertung von festigkeitshypothesen für kombinierte statische und schwingendesowiesynchrone schwingende beanspruchung. In: *Werkstoffen*, vol. 14; 1983.
- [30] Bennebach M. Fatigue multiaxiale d'une fonte GS, influence de l'entaille et d'un traitement thermique. PhD thesis, ENSAM CER de Bordeaux; 1993.
- [31] Bedkowsky W. Determination of the critical plane and effort criterium in fatigue life evaluation for material under multiaxial random loading. Experimental verification based on fatigue test of cruciform specimens. In: 4th Int conf on biaxial and multiaxial fatigue. France: ESIS; 1994. p. 435–447.
- [32] Lachowicz C, Lagoda T, Macha E, Dragon A, Petit J. Selection of algorithms for fatigue life calculation of elements made of 10HNP steel under uniaxial random loadings. *Studia Geotech Mech* 1996;18(1–2):19–43.
- [33] Lagoda T, Macha E, Bedkowsky W. A critical based approach on energy concept: application to biaxial random tension-compression high cycle fatigue regime. *Int J Fatigue* 1999;21:431–43.
- [34] Lagoda T, Macha E, Pawliczek R. The influence of mean stress on fatigue life of 10HNP steel under random loading. *Int J Fatigue* 2001;23:283–91.
- [35] Kunt M. *Traitement numérique des signaux, Traité d'électricité*, vol. 20. Presses Polytechniques et Universitaires Romandes; 1996.
- [36] Gassner E. Fatigue resistance of various materials under random loading. In: 9th ICAF symposium LBF-TR-136; 1977. p. S.3.5/1.34.
- [37] Pluvinage G. Notch effect in high cycle fatigue. In: *ICF 9 proceedings*, vol. 3; 1997. p. 1239–50.
- [38] Crossland B. Effect of large hydrostatic pressure on the torsional fatigue strength of an alloy steel. In: *International conference on fatigue of metals*. London, 1959b. p. 138–49.
- [39] Papadopoulos I. A selective review of high-cycle fatigue criteria with application in out-of-phase bending and torsion. *Eng Against Fatigue* 1999:399–406.
- [40] Nolte F, Paysan B. Dauerfestigkeitsuntersuchungen an stahlwellen bei umlaufender biege. *Verdrehbeanspruchung*; 1973.